Hybrid Active-Passive Reconfigurable Intelligent Surface-Assisted UAV Communications

Nhan T. Nguyen*, V.-Dinh Nguyen†, Qingqing Wu‡, Antti Tölli*, Symeon Chatzinotas†, and Markku Juntti*
*Centre for Wireless Communications, University of Oulu, P.O.Box 4500, FI-90014, Finland
†Interdisciplinary Centre for Security, Reliability and Trust (SnT), University of Luxembourg, L-1855 Luxembourg
‡State Key Laboratory of Internet of Things for Smart City, University of Macau, Macau 999078, China
{nhan.nguyen, antti.tolli, markku.juntti}@oulu.fi; {dinh.nguyen, symeon.chatzinotas}@uni.lu; qingqingwu@um.edu.mo

***Abstract*—We consider a novel hybrid active-passive reconfigurable intelligent surface (RIS)-assisted unmanned aerial vehicle (UAV) air-ground communications system. Unlike the conventional passive RIS, the hybrid RIS is equipped with a few active elements to not only reflect but also amplify the incident signals for significant performance improvement. Towards a fairness design, our goal is to maximize the minimum rate among users through jointly optimizing the location and power allocation of the UAV and the RIS reflecting/amplifying coefficients. The formulated optimization problem is nonconvex and challenging, which is efficiently solved via block coordinate descend and successive convex approximation. Our numerical results show that a hybrid RIS requires only 4 active elements and a power budget of 0 dBm to achieve an improvement of 52.08% in the minimum rate, while that achieved by a conventional passive RIS with the same total number of elements is only 18.06%.**

***Index Terms*—Hybrid active-passive RIS, UAV communications, power allocation, RIS semi-passive beamforming.**

I. Introduction

Unmanned aerial vehicles (UAVs)-enabled wireless communications have attracted much interest in the literature owing to the controllable mobility and cost-effectiveness of the UAV [1]. However, their system performance can be significantly degraded due to the blockage of line-of-sight (LoS) links and severe path loss caused by long-distance transmissions, especially in complex urban areas [2], [3]. Fortunately, these challenges can be overcome by deploying reconfigurable intelligent surfaces (RISs) in the system. RIS is a recent introduced technology allowing reflect radio waves in preferred directions to significantly improve the system performance [4]–[7]. This has motivated an increasing number of studies on RIS-aided UAV communications systems [2], [3], [8]–[14]. Most of these works focus on optimizing the system performance through joint transmission and reflecting designs. Specifically, in [2], [3], [9], a joint design of UAV's trajectory, power allocation/transmit beamforming, and RIS passive coefficients is proposed to maximize the system rate. The works [8], [11], [15] consider the secrecy rate maximization problems of RIS-aided UAV systems with the presence of eavesdroppers. The deployment of low-power consumption RISs can also improve the system energy efficiency or reduce the transmit power at the UAV under a constraint on quality of service. Motivated by this, the works [12], [14], [16] focus on minimizing the power consumption [16] and maximizing the energy efficiency [12], [14] of RIS-aided UAV communications systems. Moreover, RIS-aided non-orthogonal multiple access (NOMA) [16], [17], ultra-reliable and low-latency [18], millimeter-wave [10], and THz [13] RIS-aided UAV systems are also considered.

All the aforementioned works consider the passive RISs, wherein the passive reflecting gains are generally limited and can be easily surpassed by conventional relaying schemes [19] unless a very large number of reflecting elements are employed. In contrast, hybrid active-passive RIS architectures [20]–[25] are equipped with a few active elements, enabling both reflecting and amplifying gains simultaneously, can exploit the advantages of both the passive RIS and the relays. They can thus overcome the potential limitations of the passive RIS, especially in harsh transmission scenarios such as with low transmit power and/or severe path loss. As a result, the hybrid RIS is shown to provide significant improvement the system spectral efficiency [22], [26], secrecy rate [27], harvested energy [28], and reliability [29]. A fully active RIS with all active elements can achieve better spectral efficiency [30]–[32], which, however, requires higher power consumption and hardware cost compared to the hybrid one. In [20], [21], [33], [34], active RIS elements with RF chains also enable processing of incident signals and channel estimation.

Motivated by the above analysis, in this work, we propose deploying the hybrid active-passive RIS to assist the aerial-ground communications in UAV systems. Thanks to the signal amplification, the hybrid RIS with a small-to-moderate size can efficiently compensate for the severe path loss and blockage in the air-ground links, especially in complex urban scenarios, as well as for limited transmit power budget at the UAV. Focusing on system fairness, our goal is to maximize the minimum rate among the users (UEs) by jointly optimizing the UAV's location, power control, and RIS amplifying/reflecting coefficients. The problem is practically appealing but particularly more challenging compared to those with conventional passive RISs due to additional power constraints and amplified noise/interference caused by RIS active elements, and according to the authors' best knowledge, it has not been investigated in the literature. To overcome the challenges, we propose an efficient algorithm based on block coordinate descent (BCD) and successive approximation (SCA). Specifically, the original problem is first decomposed into subproblems, which are

978-1-6654-3540-6/22

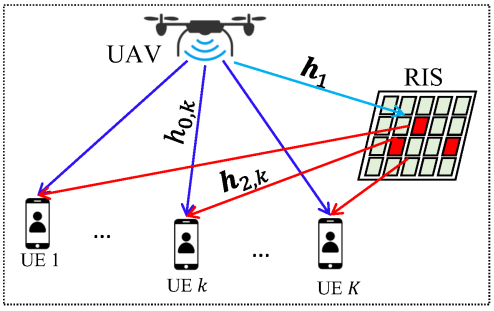

Fig. 1. Illustration of the considered hybrid RIS-aided UAV system.

then alternately solved with the SCA technique. Finally, the proposed design is evaluated by numerical results, which show that with the same total power budget, the hybrid RIS offers remarkable performance improvement compared to the systems without RIS and with the conventional passive RIS. In particular, the performance gain is more significant when the UAV's transmit power budget is limited, which typically happens in practice due to the UAV's limited battery capacity.

II. System Model and Problem Formulation

A. System Model

We consider a UAV-enabled air-ground wireless communications system, where K single-antenna UEs is served by a single-antenna UAV. A hybrid active-passive RIS with N elements is installed on a building facade to assist the air-ground communications, as illustrated in Fig. 1. We assume that $N_{\rm a}$ out of N elements are active. These active elements can potentially be realized by low-power reflection amplifiers [23], [30], which are recently introduced in [35]. The fully passive RIS with $N_{\rm a}=0$ is a special case of the hybrid RIS. Thus, in the following, we will use the general term "*RIS*" for system descriptions, and use the specific terms "*passive RIS*" or "*hybrid RIS*" for comparisons. We refer readers to [23]–[26] for more details on the implementation of the hybrid RIS.

Let $\mathcal{A}\subset\{1,2,\ldots,N\}$ be the set of the RIS active elements, $|\mathcal{A}|=N_{\rm a}$. Let α_n denote the coefficient of the nth element of the RIS, where $\alpha_n=|\alpha_n|\,e^{j\theta_n}$, with $\theta_n\in[0,2\pi)$ representing the phase shift, and $|\alpha_n|\in[0,1]$ for $n\notin\mathcal{A}$; otherwise, $|\alpha_n|\le a_{\max}$ for $n\in\mathcal{A}$. Here, $a_{\max}$ is the maximum amplitude of the active element depending on the power amplification gain of its active load, which is up to 40 dB [30], [35]. We note that the reflection amplitude of the RIS passive elements can be smaller than unity for interference cancelation in multi-user systems [7]. Let $\boldsymbol{\Upsilon}=\mathrm{diag}\{\alpha_1,\ldots,\alpha_N\}$ be the diagonal matrix of the RIS coefficients. We define an additional factorization of $\boldsymbol{\Upsilon}$ as $\boldsymbol{\Upsilon}=\boldsymbol{\Phi}+\boldsymbol{\Psi}$, where $\boldsymbol{\Psi}=\mathbb{1}_N^{\mathcal{A}}\circ\boldsymbol{\Upsilon}$ and $\boldsymbol{\Phi}=\left(\boldsymbol{I}_N-\mathbb{1}_N^{\mathcal{A}}\right)\circ\boldsymbol{\Upsilon}$ contain the active and passive coefficients, respectively. Here, $\mathbb{1}_N^{\mathcal{A}}$ is an $N\times N$ diagonal matrix whose non-zero elements are all unity and have positions determined by $\mathcal{A}$, and $\circ$ represents a Hadamard product.

Let $\boldsymbol{v}\triangleq[v_{\rm x},v_{\rm x},v_{\rm z}]^T$, $\boldsymbol{r}$, and $\boldsymbol{u}_k$ denote the locations of the UAV, the RIS, and UE k in a 3D coordinate system, respectively. We assume that the UAV flies at a fixed altitude $v_{\rm z}$, the RIS is deployed at a fixed position, and the UEs have slow mobility. Let $h_{0,k}$, $\boldsymbol{h}_1\in\mathbb{C}^{N\times1}$, and $\boldsymbol{h}_{2,k}^H\in\mathbb{C}^{1\times N}$ denote the channels UAV→UE k, UAV→RIS, and RIS→UE k, respectively, and let $\{g_{0,k},\boldsymbol{g}_1,\boldsymbol{g}_{2,k}^H\}$ be the corresponding small-scale fading channels. As a result, we can write $h_{0,k}=\zeta_0^{\frac{1}{2}}\left\|\boldsymbol{v}-\boldsymbol{u}_k\right\|^{-\frac{\epsilon_0}{2}}g_{0,k}$, $\boldsymbol{h}_1=\zeta_0^{\frac{1}{2}}\left\|\boldsymbol{v}-\boldsymbol{r}\right\|^{-\frac{\epsilon_1}{2}}\boldsymbol{g}_1$, $\boldsymbol{h}_{2,k}^H=\zeta_0^{\frac{1}{2}}\left\|\boldsymbol{r}-\boldsymbol{u}_k\right\|^{-\frac{\epsilon_2}{2}}\boldsymbol{g}_{2,k}^H$. Here, ζ_0 represents the path loss at the reference distance, i.e., 1 m, and $\{\epsilon_0,\epsilon_1,\epsilon_2\}$ are the path loss exponents. Let h_k be the effective channel between the UAV and UE k. Then, h_k can be expressed as $h_k=h_{0,k}+\boldsymbol{h}_{2,k}^H\boldsymbol{\Upsilon}\boldsymbol{h}_1$.

Denote by s_k and p_k the transmitted signal and power from the UAV to UE k, respectively, with $\mathbb{E}\{|s_k|^2\}=1$. The transmitted signal from the UAV can be given as $x=\sum_{k=1}^K\sqrt{p_k}s_k, 0\le\sum_{k=1}^K p_k\le p_{\max}^{\rm uav}$, where $p_{\max}^{\rm uav}$ is the maximum transmit power of the UAV. The received signal at UE k can be given as

$$y_k=\sqrt{p_k}h_k s_k+\sum\nolimits_{j\neq k}\sqrt{p_j}h_k s_j+\left(\boldsymbol{h}_{2,k}^H\boldsymbol{\Psi}\boldsymbol{n}_{\rm r}+n_{\rm u}\right), \quad (1)$$

where $n_{\rm u}\sim\mathcal{CN}(0,\sigma_{\rm u}^2)$ is the additive white Gaussian noise (AWGN) at UE k, and $\boldsymbol{n}_{\rm r}\sim\mathcal{CN}(\boldsymbol{0},\mathbb{1}_N^{\mathcal{A}}\circ\sigma_{\rm r}^2\boldsymbol{I}_N)$ is the total effective noise including the self-interference and AWGN noise caused by the RIS active elements operating in full-duplex mode. Thus, the term $\boldsymbol{h}_{2,k}^H\boldsymbol{\Psi}\boldsymbol{n}_{\rm r}+n_{\rm u}$ in (1) is the aggregated noise at UE k.

B. Problem Formulation

Based on (1), the achievable rate of UE k (in nats/s/Hz) can be expressed as

$$R_k=\log\left(1+\frac{p_k\left|h_k\right|^2}{\sum_{j\neq k}p_j\left|h_k\right|^2+\sigma_{\rm r}^2\|\boldsymbol{h}_{2,k}^H\boldsymbol{\Psi}\|^2+\sigma_{\rm u}^2}\right). \quad (2)$$

Let $p^{\rm ris}$ denote the transmit power of active elements of the RIS, it is constrained as $p^{\rm ris}\le p_{\max}^{\rm ris}$. Here, $p^{\rm ris}$ can be computed as $p^{\rm ris}=\mathbb{E}\{\|\boldsymbol{\Psi}(\boldsymbol{n}_{\rm r}+\boldsymbol{h}_1x)\|^2\}=\sum_{n\in\mathcal{A}}\left|\alpha_n\right|^2\xi_n$, where $\xi_n=\sigma_{\rm r}^2+\left|h_{1,n}\right|^2\sum_{k=1}^K p_k$, with $h_{1,n}$ being the nth element of $\boldsymbol{h}_1$. We aim at maximizing the minimum rate of UEs through optimizing the location and power allocation of the UAV as well as the RIS beamforming coefficients. This problem can be formulated as

$$\begin{aligned}
\underset{\boldsymbol{v},\{p_k\},\{\alpha_n\}}{\text{maximize}}\quad & \min_k\{R_k\} && \text{(3a)}\\
\text{subject to}\quad & 0\le\sum\nolimits_{k=1}^K p_k\le p_{\max}^{\rm uav}, && \text{(3b)}\\
& 0\le\theta_n\le2\pi,\ \forall n, && \text{(3c)}\\
& |\alpha_n|\le1,\ \forall n\notin\mathcal{A}, && \text{(3d)}\\
& |\alpha_n|\le a_{\max},\ \forall n\in\mathcal{A}, && \text{(3e)}\\
& \sum\nolimits_{n\in\mathcal{A}}\left|\alpha_n\right|^2\xi_n\le p_{\max}^{\rm ris}, && \text{(3f)}
\end{aligned}$$

where constraints (3c)–(3f) are design constrains of the RIS. Note in (3e) that is only active elements ($n\in\mathcal{A}$) can amplify the signals with amplification gains restricted by $a_{\max}$ [30]. Problem (3) is nonconvex, and the optimization of $\{\boldsymbol{v},\{p_k\},\{\alpha_n\}\}$ are strongly coupled in the objective function as well as constraint (3f). To overcome these challenges, we propose an efficient solution in the next section.

III. Proposed Design

We first introduce variable τ and arrive at the epigraph form of (3) as

$$\begin{aligned} \underset{\tau,\boldsymbol{v},\{p_k\},\{\alpha_n\}}{\text{maximize}} \quad & \tau && \text{(4a)} \\ \text{subject to} \quad & R_k \geq \tau, \ \forall k, && \text{(4b)} \\ & \text{(3b)} - \text{(3f)}. && \text{(4c)} \end{aligned}$$

We utilize the BCD approach and decouple (4) into three subproblems, regarding UAV's power control, UAV's location optimization, and RIS beamforming design, which are elaborated in the following subsections.

A. UAV Power Control

With given $\{\boldsymbol{v}, \{\alpha_n\}\}$, the power control can be obtained by solving problem

$$\underset{\tau,\{p_k\}}{\text{maximize}} \ \tau, \ \text{subject to (3b), (3f), (4b)}, \tag{5}$$

where (3b) and (3f) are convex, but (4b) is not. To overcome this, we first rewrite R_k in (2) as

$$R_k = \log\Big(\sum\nolimits_{j=1}^{K} p_j \left|h_k\right|^2 + \sigma_k^2\Big) - \bar{r}_k, \tag{6}$$

where $\sigma_k^2 \triangleq \sigma_{\mathrm{r}}^2 \|\boldsymbol{h}_{2,k}^H \boldsymbol{\Psi}\|^2 + \sigma_{\mathrm{u}}^2$ is constant with $\{p_k\}$, and $\bar{r}_k \triangleq \log(\sum_{j\neq k} p_j \left|h_k\right|^2 + \sigma_k^2)$. Now, constraint (4b) can be rewritten as $\log\Big(\sum_{j=1}^{K} p_j \left|h_k\right|^2 + \sigma_k^2\Big) \geq \tau + \bar{r}_k, \forall k$, where $\bar{r}_k$ is concave with $\{p_j\}_{j\neq k}$. By the first-order Taylor approximation around $\{p_j^{(i)}\}_{j\neq k}$, an upper bound of $\bar{r}_k$ can be found as

$$\bar{r}_k \leq \bar{r}_{\mathrm{ub},k}^{(i)} \triangleq \log(\tilde{p}_k^{(i)}) + \frac{1}{\tilde{p}_k^{(i)}} \sum_{j\neq k} \left|h_k\right|^2 (p_j - p_j^{(i)}). \tag{7}$$

where $\tilde{p}_k^{(i)} \triangleq \sum_{j\neq k} p_j^{(i)} \left|h_k\right|^2 + \sigma_k^2$. As a result, constraint (4b) can be approximated as

$$\log\Big(\sum\nolimits_{j=1}^{K} p_j \left|h_k\right|^2 + \sigma_k^2\Big) \geq \tau + \bar{r}_{\mathrm{ub},k}^{(i)}, \forall k. \tag{8}$$

Finally, we can approximate problem (5) by the following convex program at iteration i:

$$\underset{\tau,\{p_k\}}{\text{maximize}} \ \tau, \ \text{subject to (3b), (3f), (8)}. \tag{9}$$

B. Optimization of RIS Coefficients

Given $\{\boldsymbol{v}, \{p_k\}\}$, the coefficients of the RIS, i.e., $\{\alpha_n\}$, can be optimized by solving the following problem:

$$\underset{\tau,\{\alpha_n\}}{\text{maximize}} \ \tau, \ \text{subject to (3c)} - \text{(3f), (4b)}. \tag{10}$$

It is easy to see that constraints (3c)-(3f) are convex with respect to $\{\alpha_n\}$, but (4b) is not. Furthermore, variable $\{\alpha_n\}$ has not been exposed in the current form of (4b). As the first step to solve problem (10), we express R_k as a function of $\{\alpha_n\}$ in the following derivations. First, we can write the signal-to-interference-plus-noise ratio (SINR) term in (2) as

$$\gamma_k = \frac{p_k |h_{0,k} + \boldsymbol{h}_{2,k}^H \boldsymbol{\Upsilon} \boldsymbol{h}_1|^2}{\sum_{j\neq k} p_j |h_{0,k} + \boldsymbol{h}_{2,k}^H \boldsymbol{\Upsilon} \boldsymbol{h}_1|^2 + \sigma_{\mathrm{r}}^2 \|\boldsymbol{h}_{2,k}^H \boldsymbol{\Psi}\|^2 + \sigma_{\mathrm{u}}^2}. \tag{11}$$

Let $\boldsymbol{\alpha} \triangleq [\alpha_1, \ldots, \alpha_N]^T \in \mathbb{C}^{N\times 1}$, $\tilde{\boldsymbol{H}}_{2,k} \triangleq \mathrm{diag}\{\boldsymbol{h}_{2,k}^H\} \in \mathbb{C}^{N\times N}$, and $\tilde{\boldsymbol{h}}_{12,k} \triangleq \tilde{\boldsymbol{H}}_{2,k} \boldsymbol{h}_1 \in \mathbb{C}^{N\times 1}$. Then, we obtain $h_k = h_{0,k} + \boldsymbol{\alpha}^T \tilde{\boldsymbol{h}}_{12,k}$ and $\boldsymbol{h}_{2,k}^H \boldsymbol{\Psi} = \boldsymbol{\alpha}^T \mathbb{1}_N^{\mathcal{A}} \tilde{\boldsymbol{H}}_{2,k}$. With straightforward algebraic operations, the numerator and denominator of γ_k in (11) can be expressed as $\boldsymbol{\alpha}^H \boldsymbol{Q}_k \boldsymbol{\alpha} + 2\Re\big(\boldsymbol{\alpha}^H \boldsymbol{t}_k\big) + e_k$ and $\boldsymbol{\alpha}^H \tilde{\boldsymbol{Q}}_k \boldsymbol{\alpha} + 2\Re\big(\boldsymbol{\alpha}^H \tilde{\boldsymbol{t}}_k\big) + \tilde{e}_k$, respectively, where $\boldsymbol{Q}_k \triangleq p_k \tilde{\boldsymbol{h}}_{12,k}^* \tilde{\boldsymbol{h}}_{12,k}^T$, $\boldsymbol{t}_k \triangleq p_k \tilde{\boldsymbol{h}}_{12,k}^* h_{0,k}$, $e_k \triangleq p_k \left|h_{0,k}\right|^2$, $\tilde{e}_k \triangleq \sigma_{\mathrm{u}}^2 + \sum_{j\neq k} p_j \left|h_{0,k}\right|^2$, $\tilde{\boldsymbol{Q}}_k \triangleq \sigma_{\mathrm{r}}^2 \mathbb{1}_N^{\mathcal{A}} \tilde{\boldsymbol{H}}_{2,k}^* \tilde{\boldsymbol{H}}_{2,k}^T \mathbb{1}_N^{\mathcal{A}} + \sum_{j\neq k} p_j \tilde{\boldsymbol{h}}_{12,k}^* \tilde{\boldsymbol{h}}_{12,k}^T$, and $\tilde{\boldsymbol{t}}_k \triangleq \sum_{j\neq k} p_j \tilde{\boldsymbol{h}}_{12,k}^* h_{0,k}$. Thus, $\boldsymbol{\alpha}$ is exposed in the following form of R_k:

$$R_k(\boldsymbol{\alpha}) = \log\left(1 + \frac{\boldsymbol{\alpha}^H \boldsymbol{Q}_k \boldsymbol{\alpha} + 2\Re\big(\boldsymbol{\alpha}^H \boldsymbol{t}_k\big) + e_k}{\boldsymbol{\alpha}^H \tilde{\boldsymbol{Q}}_k \boldsymbol{\alpha} + 2\Re\big(\boldsymbol{\alpha}^H \tilde{\boldsymbol{t}}_k\big) + \tilde{e}_k}\right). \tag{12}$$

With this form, we can rewrite constraint (4b) as

$$\hat{r}_k \geq \tau + r_k, \tag{13}$$

where $\hat{r}_k \triangleq \log\Big(\|\bar{\boldsymbol{Q}}_k^{\frac{1}{2}} \boldsymbol{\alpha}\|^2 + 2\Re\big(\boldsymbol{\alpha}^H \bar{\boldsymbol{t}}_k\big) + e_k\Big)$ with $\bar{\boldsymbol{Q}}_k = \boldsymbol{Q}_k + \tilde{\boldsymbol{Q}}_k$ being positive semidefinite, $\bar{\boldsymbol{t}}_k = \boldsymbol{t}_k + \tilde{\boldsymbol{t}}_k$, and $r_k \triangleq \log(\boldsymbol{\alpha}^H \tilde{\boldsymbol{Q}}_k \boldsymbol{\alpha} + 2\Re\big(\boldsymbol{\alpha}^H \tilde{\boldsymbol{t}}_k\big) + \tilde{e}_k)$. Based on the first-order Taylor approximation around $\boldsymbol{\alpha}^{(i)}$, we have $\|\bar{\boldsymbol{Q}}_k^{\frac{1}{2}} \boldsymbol{\alpha}\|^2 \geq F(\boldsymbol{\alpha}; \bar{\boldsymbol{Q}}_k, \boldsymbol{\alpha}^{(i)}) \triangleq \|\bar{\boldsymbol{Q}}_k^{\frac{1}{2}} \boldsymbol{\alpha}^{(i)}\|^2 - 2\Big(\bar{\boldsymbol{Q}}_k^{\frac{1}{2}} \boldsymbol{\alpha}^{(i)}\Big)^H \Big(\bar{\boldsymbol{Q}}_k^{\frac{1}{2}} \boldsymbol{\alpha} - \bar{\boldsymbol{Q}}_k^{\frac{1}{2}} \boldsymbol{\alpha}^{(i)}\Big)$. Thus, a lower bound of $\hat{r}_k$ is found as

$$\hat{r}_k \geq \hat{r}_{\mathrm{lb},k}^{(i)} \triangleq \log\Big(F(\boldsymbol{\alpha}; \bar{\boldsymbol{Q}}_k, \boldsymbol{\alpha}^{(i)}) + 2\Re\big(\boldsymbol{\alpha}^H \bar{\boldsymbol{t}}_k\big) + e_k\Big). \tag{14}$$

To address the nonconvexity of r_k in (13), we introduce slack variables b_k which satisfies $b_k \geq \boldsymbol{\alpha}^H \tilde{\boldsymbol{Q}}_k \boldsymbol{\alpha} + 2\Re\big(\boldsymbol{\alpha}^H \tilde{\boldsymbol{t}}_k\big)$. Then, we can find an upper bound of r_k as

$$r_k \leq r_{\mathrm{ub},k}^{(i)} \triangleq \log\Big(b_k^{(i)} + \tilde{e}_k\Big) + \frac{b_k - b_k^{(i)}}{b_k^{(i)} + \tilde{e}_k}, \tag{15}$$

by applying the first order Taylor approximation around $b_k^{(i)}$. As a result, constraint (13) can be approximated by the following set of convex constraints:

$$\begin{aligned} \hat{r}_{\mathrm{lb},k}^{(i)} &\geq \tau + r_{\mathrm{ub},k}^{(i)}, \ \forall k, && \text{(16a)} \\ b_k &\geq \boldsymbol{\alpha}^H \tilde{\boldsymbol{Q}}_k \boldsymbol{\alpha} + 2\Re\big(\boldsymbol{\alpha}^H \tilde{\boldsymbol{t}}_k\big), \ \forall k. && \text{(16b)} \end{aligned}$$

Furthermore, we can rewrite (3f) as $\boldsymbol{\alpha}^H \boldsymbol{\Xi} \boldsymbol{\alpha} \leq p_{\max}^{\mathrm{ris}}$, where $\boldsymbol{\Xi} = \mathrm{diag}\{\tilde{\xi}_1, \ldots, \tilde{\xi}_N\}$ with $\tilde{\xi}_n = \xi_n$ for $n \in \mathcal{A}$, and $\tilde{\xi}_n = 0$ for $n \notin \mathcal{A}$. Finally, problem (10) can be approximated by the following convex program at iteration i:

$$\underset{\tau,\boldsymbol{\alpha},\{b_k\}}{\text{maximize}} \ \tau, \ \text{subject to (3c)} - \text{(3f), (16a), (16b)}. \tag{17}$$

C. Optimization of the UAV's Location

With given $\{\{p_k\}, \{\alpha_n\}\}$, the UAV' location is the solution to the following problem:

$$\underset{\tau,\boldsymbol{v}}{\text{maximize}} \ \tau, \ \text{subject to (3f), (4b)}, \tag{18}$$

which is nonconvex and very challenging. To address this problem, we first expand the expression of R_k in (2) to

show the role of $\boldsymbol{v}$. Specifically, from the expressions of $\{h_{0,k}, \boldsymbol{h}_1, \boldsymbol{h}_{2,k}^H\}$ in Section II-A, we can rewrite

$$\begin{aligned} p_j \left|h_k\right|^2 &= p_j \left|h_{0,k}\right|^2 + p_j |\boldsymbol{h}_{2,k}^H \boldsymbol{\Upsilon} \boldsymbol{h}_1|^2 + 2p_j \Re(h_{0,k}^* \boldsymbol{h}_{2,k}^H \boldsymbol{\Upsilon} \boldsymbol{h}_1) \\ &= c_{0,kj} \left\|\boldsymbol{v} - \boldsymbol{u}_k\right\|^{-\epsilon_0} + c_{1,kj} \left\|\boldsymbol{v} - \boldsymbol{r}\right\|^{-\epsilon_1} \\ &\quad + c_{2,kj} \left\|\boldsymbol{v} - \boldsymbol{u}_k\right\|^{-\epsilon_0/2} \left\|\boldsymbol{v} - \boldsymbol{r}\right\|^{-\epsilon_1/2}, \end{aligned} \tag{19}$$

where $c_{0,kj} \triangleq p_j \left|g_{0,k}\right|^2 \zeta_0$, $c_{1,kj} \triangleq p_j |\boldsymbol{h}_{2,k}^H \boldsymbol{\Upsilon} \boldsymbol{g}_1|^2 \zeta_0$, and $c_{2,kj} \triangleq 2p_j \Re(g_{0,k}^* \boldsymbol{h}_{2,k}^H \boldsymbol{\Upsilon} \boldsymbol{g}_1)\zeta_0$ are constants with respect to $\boldsymbol{v}$. While $c_{0,kj}, c_{1,kj} > 0, \forall k, j$, $c_{2,kj}$ can be either positive or negative, making it very difficult to addressing the nonconvexity of (4b). Regarding this, let us introduce set of slack variables $\boldsymbol{\mathcal{V}} \triangleq \{\{\underline{v}_{0,k}\}, \{\overline{v}_{0,j}\}, \underline{v}_1, \overline{v}_1\}$ satisfying

$$\underline{v}_{0,k} \le \left\|\boldsymbol{v} - \boldsymbol{u}_k\right\|^{-\epsilon_0/2}, \ \forall k, \tag{20a}$$

$$\overline{v}_{0,j} \ge \left\|\boldsymbol{v} - \boldsymbol{u}_j\right\|^{-\epsilon_0/2}, \ \forall j, \tag{20b}$$

$$\underline{v}_1 \le \left\|\boldsymbol{v} - \boldsymbol{r}\right\|^{-\epsilon_1/2}, \tag{20c}$$

$$\overline{v}_1 \ge \left\|\boldsymbol{v} - \boldsymbol{r}\right\|^{-\epsilon_1/2}. \tag{20d}$$

Furthermore, we introduce slack variables $\{\underline{a}_k, \overline{a}_{kj}\}$ such that

$$\underline{a}_k \le \begin{cases} c_{0,kk}\underline{v}_{0,k}^2 + c_{1,kk}\underline{v}_1^2 + |c_{2,kk}|\, \underline{v}_{0,k}\underline{v}_1, & \text{if } c_{2,kk} > 0 \\ c_{0,kk}\underline{v}_{0,k}^2 + c_{1,kk}\underline{v}_1^2 - |c_{2,kk}|\, \overline{v}_{0,k}\overline{v}_1, & \text{otherwise} \end{cases}, \tag{21a}$$

$$\overline{a}_{kj} \ge \begin{cases} c_{0,kj}\overline{v}_{0,j}^2 + c_{1,kj}\overline{v}_1^2 + |c_{2,kj}|\, \overline{v}_{0,j}\overline{v}_1, & \text{if } c_{2,kj} > 0 \\ c_{0,kj}\overline{v}_{0,j}^2 + c_{1,kj}\overline{v}_1^2 - |c_{2,kj}|\, \underline{v}_{0,j}\underline{v}_1, & \text{otherwise} \end{cases}. \tag{21b}$$

Thus, (4b) is equivalent to the following set of constraints:

$$\log\Big(1 + \frac{\underline{a}_k}{\sigma_k^2 + \sum_{j\neq k} \overline{a}_{kj}}\Big) \ge \tau, \ \forall k, \tag{22}$$
$$\text{(20a)} - \text{(21b)},$$

which are still all nonconvex. To address (22), we follow a similar approximation as for (7). Specifically, we have

$$\log\Big(\sigma_k^2 + \sum\nolimits_{j\neq k} \overline{a}_{kj} + \underline{a}_k\Big) \ge \tau + \tilde{r}_{\mathrm{ub},k}^{(i)}, \ \forall k, \tag{23}$$

where $\tilde{r}_{\mathrm{ub},k}^{(i)} \triangleq \log\Big(\sigma_k^2 + \sum_{j\neq k} \overline{a}_{kj}^{(i)}\Big) + \frac{\sum_{j\neq k} \overline{a}_{kj} - \overline{a}_{kj}^{(i)}}{\sigma_k^2 + \sum_{j\neq k} \overline{a}_{kj}^{(i)}}$. In what follows, we provide some useful approximations to tackle the nonconvexity of (20a)-(21b).

Lemma 1: Consider the following concave power, quadratic, and bilinear functions: $f_{\mathtt{pow}}(x; c) \triangleq -x^c, x \in \mathbb{R}_{++}, c > 1$ or $c < 0$, $f_{\mathtt{qua}}(\boldsymbol{x}; \boldsymbol{c}) \triangleq -\left\|\boldsymbol{x} - \boldsymbol{c}\right\|^2, \boldsymbol{x}, \boldsymbol{c} \in \mathbb{C}^n$, and $f_{\mathtt{bil}}(x, y, \delta_s) \triangleq \delta_s xy, (x, y) \in \mathbb{R}_{++}^2, \delta_s = \pm 1$, respectively. Their convex upper bounds can be found by using the first-order Taylor approximations as:

$$f_{\mathtt{pow}}(x; c) \le F_{\mathtt{pow}}(x; c, x_0) \triangleq (c-1)\, x_0^c - c x_0^{c-1} x, \tag{24}$$

$$f_{\mathtt{qua}}(\boldsymbol{x}; \boldsymbol{c}) \le F_{\mathtt{qua}}(\boldsymbol{x}; \boldsymbol{c}, \boldsymbol{x}_0) \triangleq 2(\boldsymbol{c} - \boldsymbol{x}_0)^T (\boldsymbol{x} - \boldsymbol{x}_0) - \left\|\boldsymbol{x}_0 - \boldsymbol{c}\right\|^2, \tag{25}$$

$$\begin{aligned} f_{\mathtt{bil}}(x, y; \delta_s) \le F_{\mathtt{bil}}(x, y; \delta_s, x_0, y_0) &\triangleq 0.25(x + \delta_s y)^2 \\ + 0.25(x_0 - \delta_s y_0)^2 &- 0.5(x_0 - \delta_s y_0)(x - \delta_s y). \end{aligned} \tag{26}$$

By using (24)–(26), constraints (20a)-(21b) can be approximated by the following ones at iteration i:

$$\left\|\boldsymbol{v} - \boldsymbol{u}_k\right\| + F_{\mathtt{pow}}(\underline{v}_{0,k}; -2/\epsilon_0, \underline{v}_{0,k}^{(i)}) \le 0, \ \forall k, \tag{27a}$$

$$F_{\mathtt{qua}}(\boldsymbol{v}; \boldsymbol{u}_j, \boldsymbol{v}^{(i)}) \le 1/F_{\mathtt{pow}}(\overline{v}_{0,j}; 4/\epsilon_0, \overline{v}_{0,j}^{(i)}), \ \forall j, \tag{27b}$$

$$\left\|\boldsymbol{v} - \boldsymbol{r}\right\| + F_{\mathtt{pow}}(\underline{v}_1; -2/\epsilon_1, \underline{v}_1^{(i)}) \le 0, \tag{27c}$$

$$F_{\mathtt{qua}}(\boldsymbol{v}; \boldsymbol{r}, \boldsymbol{v}^{(i)}) \le 1/F_{\mathtt{pow}}(\overline{v}_1; 4/\epsilon_1, \overline{v}_1^{(i)}), \tag{27d}$$

$$\begin{aligned} &\underline{a}_k + c_{0,kk} F_{\mathtt{qua}}(\underline{v}_{0,k}; 0, \underline{v}_{0,k}^{(i)}) + c_{1,kk} F_{\mathtt{qua}}(\underline{v}_1; 0, \underline{v}_1^{(i)}) \\ &\quad + F_{\mathtt{bil}}(\underline{v}_{0,k}, \underline{v}_1; \mathrm{sgn}(c_{2,kk}), \underline{v}_{0,k}^{(i)}, \underline{v}_1^{(i)}) \le 0, \ \forall k, \end{aligned} \tag{27e}$$

$$\begin{aligned} &c_{0,kj}\overline{v}_{0,j}^2 + c_{1,kj}\overline{v}_1^2 + F_{\mathtt{bil}}(\overline{v}_{0,j}, \overline{v}_1; \mathrm{sgn}(c_{2,kj}), \overline{v}_{0,j}^{(i)}, \overline{v}_1^{(i)}) \\ &\qquad \le \overline{a}_{kj}, \ \forall k, j, \end{aligned} \tag{27f}$$

where $\mathrm{sgn}(x)$ returns the sign of $x \in \mathbb{R}$. Constraints (27a)–(27f) are convex assuming that $\epsilon_0, \epsilon_1 < 4$. Similarly, by writing $\xi_n = \sigma_{\mathrm{r}}^2 + c_{3,n}(\left\|\boldsymbol{v} - \boldsymbol{r}\right\|^{-\epsilon_1/2})^2$, where $c_{3,n} \triangleq \left|g_{1,n}\right|^2 \zeta_0 \sum_{k=1}^K p_k$ is independent of $\boldsymbol{v}$, we can rewrite (3f) equivalently as the set constraint (27d) and

$$\sum\nolimits_{n\in\mathcal{A}} \left|\alpha_n\right|^2 \Big(\sigma_{\mathrm{r}}^2 + \sum\nolimits_{k=1}^K c_{3,n}\overline{v}_1^2\Big) \le p_{\max}^{\mathrm{ris}}. \tag{28}$$

In summary, we can approximate problem (18) at iteration i by the following convex program:

$$\underset{\tau, \boldsymbol{v}, \boldsymbol{\mathcal{V}}}{\text{maximize}} \ \tau, \ \text{subject to (23), (27a)} - \text{(28)}. \tag{29}$$

We summarize the joint optimization of the power allocation and locations of the UAV and RIS reflecting/amplifying coefficients in Algorithm 1. In step 1, the initial solutions to $\{\boldsymbol{v}^{(0)}\}$, $\{p^{(0)}\}$, $\{\alpha_n^{(0)}\}$, $\{b_k^{(0)}\}$, and $\boldsymbol{\mathcal{V}}^{(0)} = \{\underline{v}_{0,k}^{(0)}, \underline{v}_1^{(0)}, \overline{v}_{0,k}^{(0)}, \overline{v}_1^{(0)}\}$ are generated. In steps 2–7, subproblems (9), (17), and (29) are alternatively solved and $\{\boldsymbol{v}^{(i)}\}$, $\{p^{(i)}\}$, $\{\alpha_n^{(i)}\}$, and $\boldsymbol{\mathcal{V}}^{(i)}$ are updated over iterations until the objective value converges. The total complexity of Algorithm 1 is $\mathcal{O}(\mathcal{I}(\sqrt{K+2}(K+1)^3 + \sqrt{N+2K+1}(N+K+1)^3 + \sqrt{K^2+4K+2}(2K+5)^3))$, where $\mathcal{I}$ is the number of iterations until convergence.

Algorithm 1 Algorithm to Solve Problem (3)

1: **Initialization:** Set $i = 0$. Generate initial values $\{\boldsymbol{v}^{(0)}\}$, $\{p^{(0)}\}$, and $\{\alpha_n^{(0)}\}$. Initialize $\{b_k^{(0)}\}$ and $\boldsymbol{\mathcal{V}}^{(0)} = \{\underline{v}_{0,k}^{(0)}, \underline{v}_1^{(0)}, \overline{v}_{0,k}^{(0)}, \overline{v}_1^{(0)}\}$ to hold the equalities in (16b) and (20a)–(20d), respectively.
2: **repeat**
3: Solve problem (9) for given $\{\boldsymbol{v}^{(i)}\}$ and $\{\alpha_n^{(i)}\}$ to obtain solution $\{p_k^\star\}$. Set $\{p_k^{(i+1)}\} = \{p_k^\star\}$.
4: Solve problem (17) with given $\{p_k^{(i+1)}\}$, $\{\boldsymbol{v}^{(i)}\}$, and $\{b_k^{(i)}\}$ to obtain solutions $\boldsymbol{\alpha}^\star$ and $\{b_k^\star\}$. Set $\boldsymbol{\alpha}^{(i+1)} = \boldsymbol{\alpha}^\star$ and $\{b_k^{(i+1)}\} = \{b_k^\star\}$.
5: Solve problem (29) with given $\{p_k^{(i+1)}\}$, $\{\alpha^{(i+1)}\}$, $\boldsymbol{\mathcal{V}}^{(i)}$ to obtain solution $\{\boldsymbol{v}^\star\}$ and $\boldsymbol{\mathcal{V}}^\star$. Set $\{\boldsymbol{v}^{(i+1)}\} = \{\boldsymbol{v}^\star\}$ and $\boldsymbol{\mathcal{V}}^{(i+1)} = \boldsymbol{\mathcal{V}}^\star$.
6: Update $i = i + 1$.
7: **until** the increase in the objective value is smaller than ε.

IV. Numerical Results

In this section, we provide numerical results to validate the performance gain of the hybrid RIS. In the simulations, we

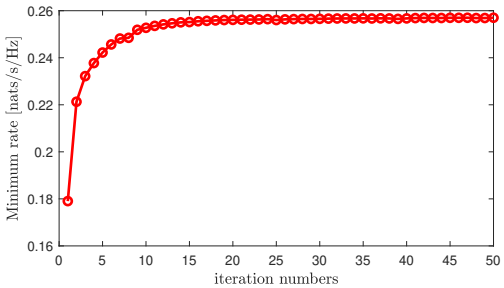

Fig. 2. Convergence of Algorithm 1 with $N = 40, p_{\max}^{\text{uav}} = 20$ dBm, $N_{\text{a}} = 2$ and $p_{\max}^{\text{ris}} = 0$ dBm.

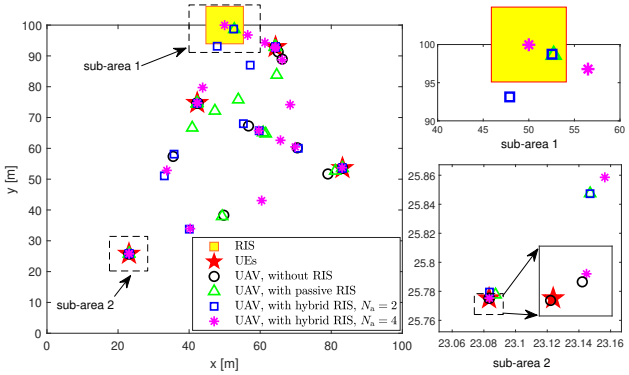

Fig. 3. Optimal locations of the UAV (for 20 channels), $N = 40$, $N_{\text{a}} = \{2, 4\}$, $p_{\max}^{\text{uav}} = 20$ dBm, and $p_{\max}^{\text{ris}} = 0$ dBm.

set $v_{\text{z}} = 100$ m, $\beta_0 = -30$ dB and $\sigma_{\text{u}}^2 = -90$ dBm, and $\sigma_{\text{r}}^2 = (\eta + 1)\sigma_{\text{u}}^2$. Here, we recall that σ_{r}^2 is the total power of noise and residual self-interference of the RIS, and $\eta = 1$ dB represents the possible residual self-interference caused by the active elements [36], [37]. We consider an area of 100×100 m^2, where $K = 4$ UEs are randomly and uniformly distributed, and the RIS is placed at $\boldsymbol{r} = [50, 100, 50]$ m. We assume Rayleigh fading channels between the UAV and UEs, deterministic LoS channel between the UAV and the RIS, and Rician fading channels between the RIS and UEs with a Rician factor of $\kappa = 10$. These are based on the fact that the LoS links between the UAV and UEs can be easily blocked by high buildings, while the RIS can be deployed at a certain height to exploit the LoS channels [2], [15], [17]. Thus, we set $\{\epsilon_0, \epsilon_1, \epsilon_2\} = \{3.2, 2.0, 2.2\}$. The positions of the RIS active elements are fixed to $\mathcal{A} = \{1, \ldots, N_{\text{a}}\}$. To solve the convex subproblems, we use modeling tool YALMIP with MOSEK solver. The convergence criteria is set to $\varepsilon = 10^{-4}$.

We first show in Fig. 2 the convergence of Algorithm 1, which is initialized as follows: First, the UAV's initial location is right above the center of the area and at the height of $v_{\text{z}} = 100$ m. The UAV's transmit power is initialized as $p_k = p_{\max}^{\text{uav}}/K, \forall k$, implying an equal power allocation to UEs. Then, the initial coefficients of the RIS are set to $\alpha_n^{(0)} = re^{j\theta_n^{(0)}}, \forall n$, where phase shifts $\{\theta_n^{(0)}\}$ are randomly generated in $[0, 2\pi)$, and r satisfies (3e) and (3f). It is observed from Fig. 2 that Algorithm 1 converges after about 20 iterations.

In Fig. 3, we plot the optimized locations (for 20 channels) of the UAV in the systems without RIS, with passive RIS, and with hybrid RIS. It is observed that in all the considered

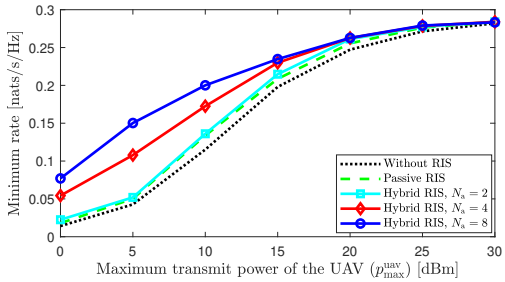

Fig. 4. Minimum rates versus UAV maximum transmit power, $N = 40, N_{\text{a}} = \{2, 4, 8\}, p_{\max}^{\text{uav}} \in [0, 30]$ dBm, $p_{\max}^{\text{ris}} = 0$ dBm.

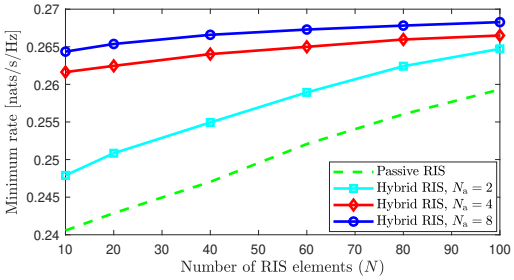

Fig. 5. Minimum rates versus numbers of RIS elements, $N \in [10, 100]$, $N_{\text{a}} = \{2, 4, 8\}$, $p_{\max}^{\text{uav}} = 20$ dBm, $p_{\max}^{\text{ris}} = 0$ dBm.

systems, the UAV flies either above one of the UEs (e.g., sub-area 2) or in between the UEs. However, with the deployment of RIS, the UAV also flies above the RIS (sub-area 1), which is not seen for the system without RISs. Furthermore, the UAV deploys near the hybrid RIS more frequently than the passive RIS. In particular, when the number of active elements in the hybrid RIS increases, the chances that the UAV flies near the RIS also increases, and there is a case that it flies right above the hybrid RIS with $N_{\text{a}} = 4$ active elements. These results on the UAV's locations show that the hybrid RIS can significantly enhance the air-ground channels so that the UAV does not necessarily always flies near or in between the UEs; it can also fly above the RIS to exploit the strong reflecting channels.

In Fig. 4, we show the minimum rates versus the UAV maximum transmit power. It is observed that both the passive and hybrid RISs offer performance improvement to the system. However, the gains of the passive RIS and hybrid RIS with $N_{\text{a}} = 2$ are limited. When the number of active elements increases, i.e., with $N_{\text{a}} = \{4, 8\}$, the hybrid RIS offers very significant performance improvement. For example, at $p_{\max}^{\text{uav}} = 10$ dBm, the passive RIS achieves an improvement of 18.06% compared to the case without RIS, while those attained by the hybrid RISs with $N_{\text{a}} = \{4, 8\}$ are $\{52.08\%, 73.61\%\}$, respectively. In particular, the gains of the hybrid RIS are more significant at low $p_{\max}^{\text{uav}}$, which generally happens in practice due to the limited capacity of the UAV's battery.

We show in Fig. 5 the minimum rates of the considered systems versus N, i.e., $N \in [10, 100]$. It is seen that as N increases, the passive RIS performs approaching the hybrid ones. In contrast, the performance improvement is not always clearly seen for the hybrid RIS. Specifically, with $N_{\text{a}} = 2$, the minimum rate increases quickly with N, but with $N_{\text{a}} = \{4, 8\}$, it increases relatively slowly because the passive reflecting gain is dominated by the active beamforming gains. Thus,

adding more passive elements does not provide significant improvement to such hybrid RISs. Furthermore, it is seen that a hybrid RIS with $N = 10$ and $N_{\mathrm{a}} = 4$ performs comparable to the passive RIS with $N = 100$.

V. Conclusion

We proposed the deployment of the hybrid active-passive RIS architecture to enhance the performance of UAV communications systems. In this hybrid RIS, a few active elements were employed to provide the RIS with both reflecting and amplifying gains. We formulated a max-min rate problem and proposed an efficient algorithm based on the BCD and SCA approaches to optimize the UAV's location, power control, and RIS amplifying/reflecting coefficients. Finally, the proposed design was evaluated through extensive numerical results. It was numerically justified that the hybrid RIS offers remarkable performance improvement compared to the systems without RIS and that with the conventional passive RIS. For future studies, RIS-aided air-ground communications systems with multiple UAVs and multi-antenna devices can be considered.

Acknowledgment

This work has been supported in part by Academy of Finland under 6G Flagship (grant 318927), EERA Project (grant 332362), and Infotech Program funded by University of Oulu Graduate School.

References

[1] Q. Wu, Y. Zeng, and R. Zhang, "Joint trajectory and communication design for multi-UAV enabled wireless networks," *IEEE Trans. Wireless Commun.*, vol. 17, no. 3, pp. 2109–2121, 2018.

[2] X. Cao *et al.*, "Reconfigurable intelligent surface-assisted aerial-terrestrial communications via multi-task learning," *IEEE J. Sel. Areas Commun.*, vol. 39, no. 10, pp. 3035–3050, 2021.

[3] S. Li, B. Duo, X. Yuan, Y.-C. Liang, and M. Di Renzo, "Reconfigurable intelligent surface assisted UAV communication: Joint trajectory design and passive beamforming," *IEEE Commun. Lett.*, vol. 9, no. 5, pp. 716–720, 2020.

[4] N. T. Nguyen *et al.*, "Machine learning-based reconfigurable intelligent surface-aided MIMO systems," in *Proc. IEEE Works. on Sign. Proc. Adv. in Wirel. Comms.*, 2021, pp. 101–105.

[5] S. Hu, F. Rusek, and O. Edfors, "Beyond massive MIMO: The potential of positioning with large intelligent surfaces," *IEEE Trans. Signal Process.*, vol. 66, no. 7, pp. 1761–1774, 2018.

[6] C. Huang *et. al*, "Reconfigurable intelligent surfaces for energy efficiency in wireless communication," *IEEE Trans. Wireless Commun.*, vol. 18, no. 8, pp. 4157–4170, 2019.

[7] Q. Wu and R. Zhang, "Towards smart and reconfigurable environment: Intelligent reflecting surface aided wireless network," *IEEE Commun. Mag.*, vol. 58, no. 1, pp. 106–112, 2019.

[8] S. Li, B. Duo, M. Di Renzo, M. Tao, and X. Yuan, "Robust secure UAV communications with the aid of reconfigurable intelligent surfaces," *IEEE Trans. Wireless Commun.*, vol. 20, no. 10, pp. 6402–6417, 2021.

[9] J. Li and J. Liu, "Sum rate maximization via reconfigurable intelligent surface in UAV communication: Phase shift and trajectory optimization," in *Proc. Int. Conf. Commun. Network. in China*, 2020, pp. 124–129.

[10] L. Jiang and H. Jafarkhani, "Reconfigurable intelligent surface assisted mmwave UAV wireless cellular networks," in *Proc. IEEE Int. Conf. Commun.*, 2021, pp. 1–6.

[11] X. Guo, Y. Chen, and Y. Wang, "Learning-based robust and secure transmission for reconfigurable intelligent surface aided millimeter wave UAV communications," *IEEE Wireless Commun. Lett.*, vol. 10, no. 8, pp. 1795–1799, 2021.

[12] M. Diamanti, M. Tsampazi, E. E. Tsiropoulou, and S. Papavassiliou, "Energy efficient multi-user communications aided by reconfigurable intelligent surfaces and UAVs," in *SMARTCOMP*, 2021, pp. 371–376.

[13] Y. Pan, K. Wang, C. Pan, H. Zhu, and J. Wang, "UAV-assisted and intelligent reflecting surfaces-supported terahertz communications," *IEEE Wireless Commun. Lett.*, vol. 10, no. 6, pp. 1256–1260, 2021.

[14] K. K. Nguyen, *at. al*, "Reconfigurable intelligent surface-assisted multi-uav networks: Efficient resource allocation with deep reinforcement learning," *IEEE J. Sel. Topics Signal Process.*, 2021.

[15] J. Li, S. Xu, J. Liu, Y. Cao, and W. Gao, "Reconfigurable intelligent surface enhanced secure aerial-ground communication," *IEEE Trans. Wireless Commun.*, vol. 69, no. 9, pp. 6185–6197, 2021.

[16] X. Liu, Y. Liu, and Y. Chen, "Machine learning empowered trajectory and passive beamforming design in uav-ris wireless networks," *IEEE J. Sel. Areas Commun.*, 2020.

[17] X. Mu, Y. Liu, L. Guo, J. Lin, and H. V. Poor, "Intelligent reflecting surface enhanced multi-UAV NOMA networks," *IEEE J. Sel. Areas Commun.*, 2021.

[18] A. Ranjha and G. Kaddoum, "URLLC facilitated by mobile UAV relay and RIS: A joint design of passive beamforming, blocklength, and UAV positioning," *IEEE Internet Things J.*, vol. 8, no. 6, pp. 4618–4627, 2020.

[19] E. Björnson, O. Özdogan, and E. G. Larsson, "Intelligent reflecting surface vs. decode-and-forward: How large surfaces are needed to beat relaying?" *IEEE Wireless Commun. Lett.*, vol. 9, no. 2, pp. 244–248, 2019.

[20] A. Taha, M. Alrabeiah, and A. Alkhateeb, "Deep learning for large intelligent surfaces in millimeter wave and massive MIMO systems," in *IEEE Global Commun. Conf. (GLOBECOM)*, 2019, pp. 1–6.

[21] G. C. Alexandropoulos and E. Vlachos, "A hardware architecture for reconfigurable intelligent surfaces with minimal active elements for explicit channel estimation," in *Proc. IEEE Int. Conf. Acoust., Speech, Signal Processing*, 2020, pp. 9175–9179.

[22] N. T. Nguyen, Q.-D. Vu, K. Lee, and M. Juntti, "Spectral efficiency optimization for hybrid relay-reflecting intelligent surface," *Proc. IEEE Int. Conf. Commun. Workshop*, 2021.

[23] ——, "Hybrid relay-reflecting intelligent surface-assisted wireless communication," *arXiv preprint arXiv:2103.03900*, 2021.

[24] N. T. Nguyen *et al.*, "Hybrid relay-reflecting intelligent surface-aided wireless communications: Opportunities, challenges, and future perspectives," *arXiv preprint arXiv:2104.02039*, 2021.

[25] A. Shojaeifard *et al.*, "MIMO evolution beyond 5G through reconfigurable intelligent surfaces and fluid antenna systems," *Proc. IEEE*, 2022.

[26] N. T. Nguyen *et al.*, "Downlink throughput of cell-free massive MIMO systems assisted by hybrid relay-reflecting intelligent surfaces," in *Proc. IEEE Int. Conf. Commun.*, 2022.

[27] K.-H. Ngo *et al.*, "Low-latency and secure computation offloading assisted by hybrid relay-reflecting intelligent surface," in *IEEE Int. Conf. Advanced Tech. Commun. (ATC)*, 2021, pp. 306–311.

[28] S. Ahmed, A. E. Kamal, and M. Y. Selim, "Adding active elements to reconfigurable intelligent surfaces to enhance energy harvesting for IoT devices," in *IEEE Military Commun. Conf.*, 2021, pp. 297–302.

[29] Z. Yigit, E. Basar, M. Wen, and I. Altunbas, "Hybrid reflection modulation," *arXiv preprint arXiv:2111.08355*, 2021.

[30] R. Long, Y.-C. Liang, Y. Pei, and E. G. Larsson, "Active reconfigurable intelligent surface aided wireless communications," *IEEE Trans. Wireless Commun.*, 2021.

[31] M. H. Khoshafa *et. al*, "Active reconfigurable intelligent surfaces-aided wireless communication system," *IEEE Commun. Lett.*, vol. 25, no. 11, pp. 3699–3703, 2021.

[32] G. Chen *et. al*, "Active IRS aided multiple access for energy-constrained IoT systems," *arXiv preprint arXiv:2201.12565*, 2022.

[33] R. Schroeder, J. He, and M. Juntti, "Passive RIS vs. Hybrid RIS: A comparative study on channel estimation," in *Proc. IEEE Veh. Technol. Conf.*, June 2021, pp. 1–7.

[34] J. He *et al.*, "Channel estimation and hybrid architectures for ris-assisted communications," in *Joint European Conf. Netw. Commun. & 6G Summit*. IEEE, 2021, pp. 60–65.

[35] N. Landsberg and E. Socher, "A low-power 28-nm CMOS FD-SOI reflection amplifier for an active F-band reflectarray," *IEEE Trans. Microw. Theory Techn.*, vol. 65, no. 10, pp. 3910–3921, 2017.

[36] R. Malik and M. Vu, "Optimal transmission using a self-sustained relay in a full-duplex MIMO system," *IEEE J. Sel. Areas Commun.*, vol. 37, no. 2, pp. 374–390, 2018.

[37] D. Bharadia and S. Katti, "Full duplex MIMO radios," in *11th USENIX Symp. Netw. Syst. Design Implement. (NSDI)*, 2014, pp. 359–372.